


Unsupervised PolSAR Change Detection Based on Polarimetric Distance Measurements and ConvLSTM Network

Rong Gui , Xinyue Zhang , Jun Hu , Senior Member, IEEE, Lei Wang , and Xing Zhang 

Abstract—Time-series PolSAR are capable for continuous change monitoring of natural resources and urban land-covers regardless of weather and lighting conditions. However, in the big SAR data era, the scarcity of labeled PolSAR samples poses new challenge to the traditional change detection methods. To reduce the dependence on labeled samples and ensure the efficiency of long time-series PolSAR interpretation, an unsupervised and pseudolabel-based change detection method is proposed. First, the similarity maps of time-series PolSAR are gauged by three selected polarimetric distance measurements (PDMs), which are suitable for PolSAR distribution characteristics and have the potential to reflect PolSAR changes. Second, the high-confidence changed pseudosamples are selected based on the similarity maps, and the unchanged pseudosamples are selected based on the nonsimilarity maps. Third, the limited selected pseudosamples (changed and unchanged) and multidimensional features are used to train the ConvLSTM network for change detection, and the input features include the T_3 coherence matrix elements of time-series PolSAR and the aforementioned PDMs. Finally, the change detection results based on pseudosamples and the ConvLSTM network can be obtained, without additional manual labels. Adequate experiments are conducted on Radarsat-2, UAVSAR full-polarized, and Sentinel-1 dual-polarized datasets, achieving improved unsupervised change detection accuracy at 89.59–93.24%.

Index Terms—Long short-term memory (LSTM) network, polarimetric distance measurements (PDMs), synthetic aperture radar (SAR), time series images, unsupervised change detection.

I. INTRODUCTION

CHANGE detection is a well-established field in remote sensing image interpretation. The definition of change

Manuscript received 15 July 2023; revised 13 September 2023; accepted 13 October 2023. Date of publication 17 October 2023; date of current version 27 October 2023. This work was supported in part by the National Natural Science Foundation of China under Grant 42201432 and Grant 42030112, in part by the Nature Science Foundation of Hunan Province under Grant 2022JJ40631 and Grant 2020JJ2043, in part by the Project of Innovation-driven Plan of Central South University under Grant 2023ZZTS0758. (Corresponding author: Jun Hu.)

Rong Gui and Jun Hu are with the School of Geosciences and Info-physics, Central South University, Changsha 410083, China, and also with the Key Laboratory of Metallogenic Prediction of Nonferrous Metals and Geological Environment Monitoring (Central South University), Ministry of Education, Changsha 410083, China (e-mail: ronggui@csu.edu.cn; csuhujun@csu.edu.cn).

Xinyue Zhang and Xing Zhang are with the School of Geosciences and Info-Physics, Central South University, Changsha 410083, China (e-mail: xinyuezhang@csu.edu.cn; lzxzhangxing@csu.edu.cn).

Lei Wang is with the School of Electrical and Information Engineering, Wuhan Institute of Technology, Wuhan 430079, China (e-mail: wanglei2016@whu.edu.cn).

Digital Object Identifier 10.1109/JSTARS.2023.3325370

detection is to identify changes between time-series images. Such technology has been first established in the satellites with optical sensors, and been widely used in urban and rural planning [1], [2], agricultural management [3], disaster emergencies [4], [5], and other fields [6]. With the rapid development of airborne and spaceborne synthetic aperture radar (SAR) systems, an extensive and worldwide repository of time-series SAR image data has been accumulated. Because the SAR system equips with active imaging sensor in microwave band, it enables weather-independent ability for the change detection. Although the scattering information contains in multidimensional dual-polarization, and full-polarization time-series SAR data can reflect the long-term dynamic changes of the land-covers, corresponding research is still in an early age [7].

Deep learning is a machine learning model driven by Big Data. The deep learning method can automatically extract the quantitative expression of features from raw data, thereby enabling the real-world tasks such as pattern recognition. Typical deep learning networks, such as CNN [8], [9], RNN [10], recent Transformer [2], and their derivatives such as Unet [11], Ms-CapsNet [12], ShearNet [10], have been involved in supervised SAR change detection tasks. These supervised deep learning network have outperformed in SAR temporal data change detection. However, the accurate construction of supervised deep learning models depends on large-scale training labels, while limited annotated dataset is available [13], [14]. Obviously, the efficiency of manual annotation is label tedious, thereby impeding the efficient and high-precision interpretation of time-series SAR images.

Therefore, considering the dependence of supervised methods on annotated samples, how to automatically obtain changing information of land-cover from time-series SAR data under unsupervised conditions is an important issue in current SAR interpretation research [15], [16]. Compared to supervised methods, unsupervised change detections do not require labeled samples, and can obtain SAR change information more quickly and conveniently. However, traditional unsupervised methods are difficult to discover the variation patterns contained in massive time-series SAR data. Thus, the accuracy of traditional unsupervised methods is always lower than that of supervised methods. Deep learning is beneficial for discovering the changing patterns of massive time-series data. Therefore, combining advanced deep learning algorithms to explore efficient unsupervised change

detection networks will be a key research direction for future deep learning interpretation methods of PolSAR images.

To achieve an effective and generalized PolSAR change detection method under unsupervised conditions, this article proposes a method for generating changing/un-changing pseudolabels in time-series PolSAR data and an innovate unsupervised PolSAR change detection method rooted on the new generation of changing/un-changing pseudolabels in time-series PolSAR data and polarimetric similarity and long short-term memory (LSTM) network. The proposed method has the following novelty and contributions.

- 1) An unsupervised change detection method based on polarimetric feature similarity and LSTM network is proposed, achieving both generalization and efficiency accuracy.
- 2) The reliance of manual labeled samples has been extensively decreased using the pseudolabel strategy, and enabling its unsupervised application to time-series PolSAR data rather than the dual time series.
- 3) The potential change factor evaluation indicators for time-series PolSAR have been validated, facilitating the rapid identification of potential changing sites.

The rest of this article is organized as follows. In Section II, the domain shifts problem between time-series PolSAR images and related change detection works are documented. In Section III, the proposed polarimetric distance measurements (PDM)-LSTM framework is presented. Section IV describes the datasets, the experimental settings, and the results and discussion. Finally, Section V concludes this article.

II. DOMAIN SHIFTS PROBLEM AND RELATED WORKS

A. Domain Shifts Problem in Time-Series PolSAR Images

Commonly, there is a significant domain shifts problem among time-series PolSAR data. This problem arises from the side looking imaging mode and multiple acquisition times. As shown in Fig. 1, two fully polarized data sensed by Radarsat-2 shows a significant domain shift problems of polarimetric feature among samples in the same region. This varying domain shifts problem hinders the reuse of labeled samples between time series PolSAR images. That is to say, the existing annotated PolSAR samples cannot be applied to the subsequent data directly. Moreover, the domain adaptive transfer learning methods for optical images may not be suitable for PolSAR image data either.

This domain shifts problem indicates that the accumulated historical labeled samples are difficult to be effective in recent temporal data. Moreover, varying degrees of domain shifts in time series data can also make it difficult to reuse labeled samples. Therefore, obtaining change detection results of PolSAR time series data by unsupervised manner is necessary. It is worth noting that even though there has feature differences between multitemporal PolSAR images, a certain degree of similarity also exists. Inspired by this similarity, this article intends to express the measurements of change and nonchange information between time-series PolSAR through the similarity of polarimetric features. By utilizing polarimetric feature similarity and

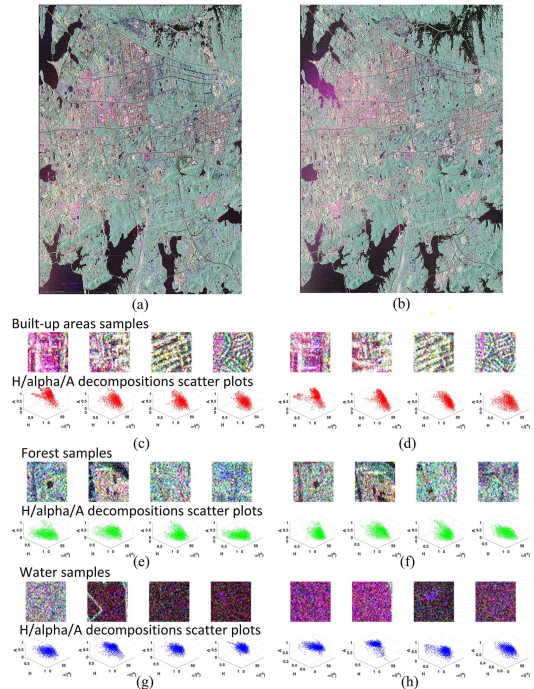


Fig. 1. Pseudocolor images of time-series PolSAR data, and corresponding H/alpha/A scattering maps of different land-covers, (a) and (b) are the Pauli RGB images for radarsat-2 datasets of wuhan region in 2011 and 2015, (c) and (d) are the H/alpha/A scatterings of building areas in (a) and (b); (e) and (f) are the H/alpha/A scatterings of vegetation areas in (a) and (b); (g) and (h) are the H/alpha/A scatterings of water areas in (a) and (b).

unsupervised methods to avoid the influence of domain shifts indirectly, a more widely applicable change detection method for PolSAR time-series is studied.

B. Unsupervised Change Detection Methods for SAR Images

With the continuous development of earth observation technology and artificial intelligence technology, the methods applied to SAR image change detection are also continuously developing and improving. These change detection methods can be classified and summarized according to different classification standards. Depending on the necessity of prior data, SAR change detection methods can be divided into unsupervised methods and supervised methods. The supervised change detection method provides accurate guidance information from both raw and given data. It is often possible to obtain a highly representative and distinguishable combination of feature information. Therefore, the detection accuracies of the supervised methods outperform the unsupervised methods, typically. However, in most change detection application scenarios, prior data of the target area is difficult to be obtained or requires significant human efforts. Consequently, most change detection scenarios lack effective or sufficient labeled sample data for supervised learning. At this point, the unsupervised methods can play an important role. The main steps of unsupervised change detection methods are as follows: 1) Preprocessing such as registration and geometric correction; 2) difference map generation; 3) difference graph analysis processing (threshold segmentation or clustering) [17]. Unsupervised change detection methods can be divided into two

types: object-based and pixel-based. Object-based methods include method based on binary tree segmentation, method based on hyperpixel segmentation, wishart hybrid model method, and extended region statistical fusion method. Pixel-based methods include difference method, ratio method, logarithmic ratio method, change vector analysis method, and principal component analysis method.

Pixel-based change detection methods take pixel points as the unit of analysis, perform difference analysis on high-dimensional features, and ultimately generate a change map. Zhang et al. [18] extracted patches around pixels from images of different time periods as spatial neighborhood features of pixels, and used unsupervised deep belief networks to obtain high-dimensional features of the pair of patches. Then, the cosine distance and change intensity of the high-dimensional features of the two images are calculated, and the changing pixel points and nonchanging pixel points are distinguished through a two-dimensional polarization domain analysis method. Gao et al. [19] established a very DCNet to utilize discriminant features, and introduced residual learning and fusion mechanisms to solve the exploding gradients problem. Gao et al. [20] introduced dual-tree complex wavelet transform in convolutional-wavelet neural networks (CWNNs) to effectively reduce the effect of speckle noise, and employ a virtual sample generation scheme to create samples for CWNN training for the problem of limited samples.

Object-based change detection method detects changes on an object-by-object basis based on the segmented object, and segments the high-dimensional features of the object extracted from the deep learning network. Lv et al. [21] used a simple linear clustering method to segment hyperpixels, then used a compression codec to extract high-dimensional features from hyperpixels, and finally used the K -means clustering method to classify and detect changing and nonchanging categories of hyperpixels. Lei et al. [22] proposed a novel change detection technique based on multiscale super pixel segmentation and stacked denoising autoencoders. This approach is designed to achieve super pixel-based change detection, in which the basic analysis unit is between pixel-based and object-based ones. Recently, research works proposed some new change detection methods such as hybrid change detection method. Lu et al. [5] proposed a new unsupervised algorithm-level fusion scheme to improve the accuracy of Pixel-based change detection using spatial context information through object-based change detection approach.

The above unsupervised change detection methods are usually not highly automated and inaccurate, but with a wide application to most SAR data. To enhance the automation and efficiency of unsupervised time-series PolSAR data, this article aims to utilize polarimetric similarity and deep learning to improve the efficiency and accuracy of unsupervised change detection for PolSAR data.

C. Application of LSTM Network in Remote Sensing Image Interpretation

The basis of SAR image change detection is the time-series data. The recurrent neural network (RNN) can combine two

temporal data through cyclic hiding states to extract temporal correlation information from dual temporal data, making full use of the temporal correlation characteristics of time series data. The RNN has more advantages than CNN in processing sequence data with interdependence. Due to the difficulty of RNN in learning the feature representation of long sequences, the LSTM network was proposed by improving the cyclic structure of RNN [23]. The training errors in the LSTM network propagate over a time sequence to capture the time-dependent relation of historical information on training data. The LSTM network can extract characteristic time series curves from remote sensing images, demonstrating excellent performance in SAR image interpretation tasks.

Recently, Wang et al. [24] proposed a multiview attention convolutional neural network with LSTM network to extract and fuse the features from SAR images with adjacent azimuths. Zhou et al. applied a LSTM model to quantify the relations between tobacco's phenological information and the phenological features extracted from time series S1-A SAR data, demonstrating the potential of LSTM network in using time series S1-A SAR data to map crop cultivation [3]. Lin et al. [25] proposed a change type recognition method for SAR images based on a statistical bidirectional LSTM network. This model produced high-quality results under small sample on two sets of medium-to-low resolution SAR image data and one set of GaoFen-3 high-resolution real SAR image data.

To fully utilize the high-dimensional features and polarimetric similarity of time-series PolSAR data, the LSTM network is chosen as the framework in this article.

III. METHODS

The workflow of proposed PDM-ConvLSTM framework is shown in Fig. 2. First, the similarity maps of time-series PolSAR are calculated, including the three selected typical PDMs, which are used to evaluate the similarity and nonsimilarity of time-series PolSAR. Second, the high-confidence changed pseudosamples are selected based on the similarity maps, and the unchanged pseudosamples are selected based on the nonsimilarity maps. Third, the selected pseudosamples (changed and unchanged) are used to train LSTM network for change detection, and the input features include the T_3 elements of time-series PolSAR and the above three distance measurement features. Finally, the change detection results based on pseudosamples and LSTM network can be obtained, without additional manual labels.

A. Applied Polarimetric Similarity Metrics

Similarity measurement based on the polarimetric metric can be used to determine the similarity of time-series PolSAR images. The steps of determining the similarity of time-series PolSAR images include calculating the difference maps and automatically determining the similarity thresholds. Distance measurement can measure the similarity of time-series images and plays a crucial role in various applications of PolSAR image data. The distance measures can be used to measure the degree of change between PolSAR in change detection [26].

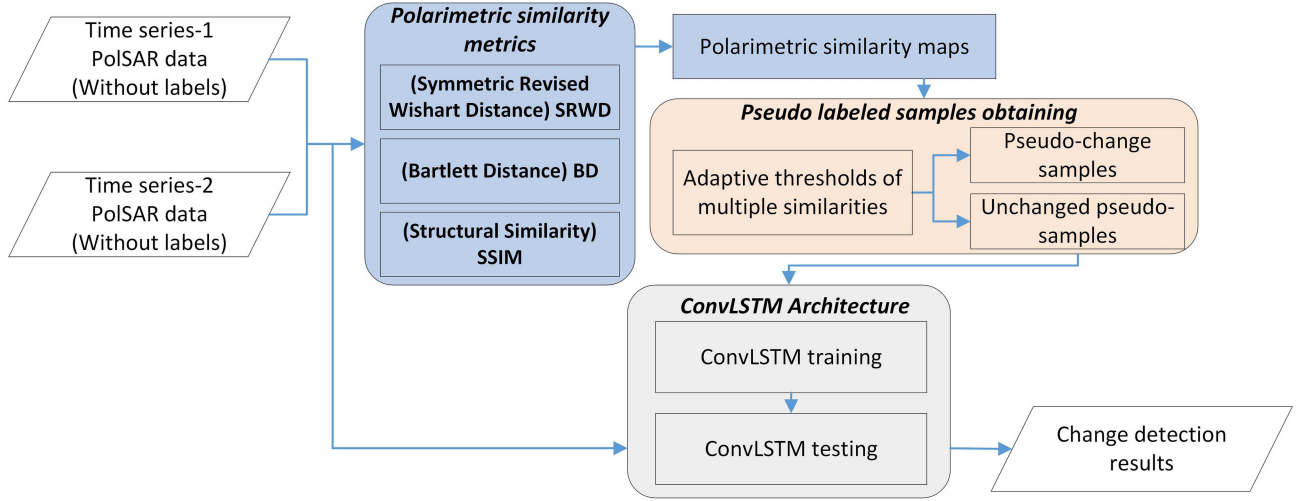


Fig. 2. Flowchart of the proposed PDM-ConvLSTM framework.

1) *Symmetric Revised Wishart Distance*: Revised Wishart distance d_{RW} has been widely used in previous studies [27], [28], and defined as follows:

$$d_{RW}(T_i, T_j) = -\ln \frac{|T_j|}{|T_i|} + \text{tr}(T_j^{-1}T_i) - d \quad (1)$$

where $\text{tr}(\cdot)$ denotes the trace operation, d is the dimension of scattering vector, and T_i and T_j are the coherence matrices for time-series PolSAR image i and j , respectively.

Considering the symmetry of the revised Wishart distance, a revised Wishart distance d_{SRW} is introduced and defined as follows [29]:

$$\begin{aligned} d_{SRW}(T_i, T_j) &= \frac{d_{RW}(T_i, T_j) + d_{RW}(T_j, T_i)}{2} \\ &= \frac{\text{tr}(T_i T_j^{-1} + T_j T_i^{-1})}{2} - d \end{aligned} \quad (2)$$

where $d_{RW}(\cdot)$ is the revised Wishart distance.

Ren et al. [30] incorporate the weight adjacency matrix to perform weighted graph convolution based on the symmetric revised Wishart distance, which describes the similarity between the neighboring pairwise superpixels.

2) *Bartlett Distance*: Bartlett distance can capture street lattice and building structures, and perform well for double-bounce objects. The similarity measure called the Bartlett distance is defined as follow [28]:

$$d_B(T_i, T_j) = \log \frac{|T_{i+j}|}{|T_i|} + \log \frac{|T_{i+j}|}{|T_j|} = 2 \log \frac{|T_{i+j}|}{\sqrt{|T_i||T_j|}} \quad (3)$$

where T_i and T_j are the coherence matrices for time-series PolSAR image i and j , respectively, and $T_{i+j} = \frac{1}{2}T_i + \frac{1}{2}T_j$.

3) *Structural Similarity Index Measure*: The structural similarity index measure (SSIM) is used to measure the similarity between two given images. SSIM mainly considers three key characteristics of images: luminance $l(x, y)$, contrast $c(x, y)$, and structure $s(x, y)$ [31]. The time-series PolSAR images are

converted into grayscale images after Pauli RGB decomposition, as the input images x, y .

The measured values of the above three characteristics are represented as follows:

$$l(x, y) = \frac{2\mu_x\mu_y + C_1}{\mu_x^2 + \mu_y^2 + C_1} \quad (4)$$

where $\mu_x = \frac{1}{N} \sum_{i=1}^N x_i$, $C_1 = (K_1L)^2$, L is the grayscale progression of the image, and $K1 \ll 1$.

$$c(x, y) = \frac{(2\sigma_x\sigma_y + C_2)}{(\sigma_x^2 + \sigma_y^2 + C_2)} \quad (5)$$

where $\sigma_x = \sqrt{\frac{1}{N-1} \sum_{i=1}^N (x_i - \mu_x)^2}$, $C_2 = (K_2L)^2$, and $K2 \ll 1$.

$$s(x, y) = \frac{\sigma_{xy} + C_3}{\sigma_x\sigma_y + C_3} \quad (6)$$

where $\sigma_x \sigma_y = \frac{1}{N-1} \sum_{i=1}^N (x_i - \mu_x)(y_i - \mu_y)$.

Combine $l(x, y)$, $c(x, y)$, and $s(x, y)$ to obtain $SSIM(x, y)$:

$$SSIM(x, y) = l(x, y)^\alpha \cdot c(x, y)^\beta \cdot s(x, y)^\gamma \quad (7)$$

where α, β, γ , respectively, represent the proportion of different features in SSIM. When $\alpha = \beta = \gamma = 1$ and $C3 = C2/2$

$$SSIM(x, y) = \frac{(2\mu_x\mu_y + C_1)(2\sigma_x\sigma_y + C_2)}{(\mu_x^2 + \mu_y^2 + C_1) * (\sigma_x^2 + \sigma_y^2 + C_2)} \quad (8)$$

There are two main motivations for selecting these three PDMs. First, the selected distance measures need to be suitable for polarimetric features. Due to the special distribution characteristics of polarimetric features, not all distance measures are suitable for polarimetric data. In addition, the measure maps obtained by the selected distances should have good correlation with the PolSAR change and nonchange areas, which means the selected distances should be potential benefit to reflect PolSAR changes. The three distance measures introduced abovementioned that are suitable for describing polarimetric matrices can

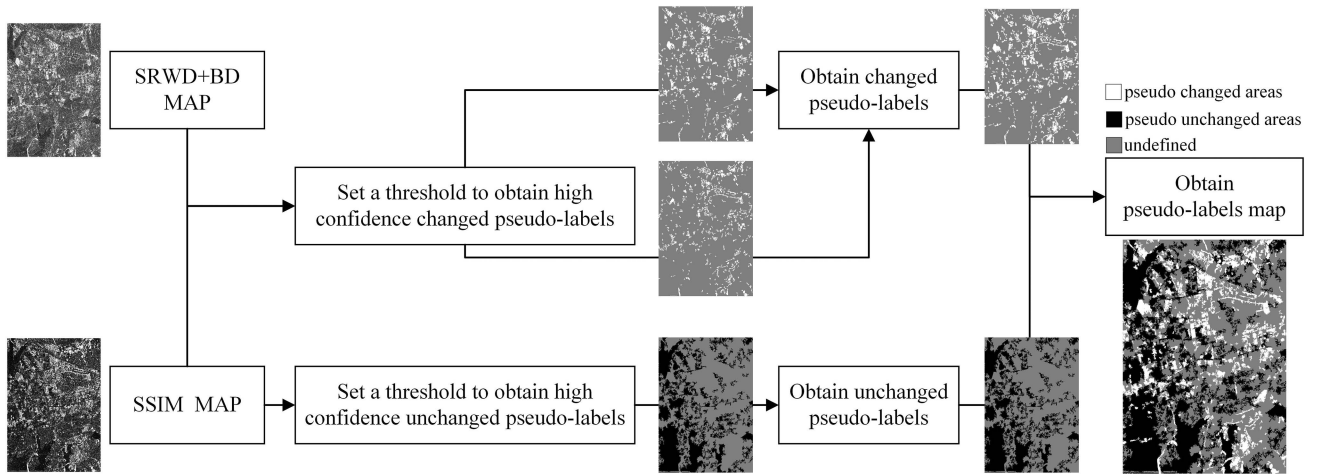


Fig. 3. Process of obtaining pseudolabels map.

be used to obtain similarity and dissimilarity maps between time-series PolSAR data. Here, because SRWD and BD distance measure maps are more likely to reflect the difference of the change region, this article mainly uses them to determine the difference measure map between the two-time PolSAR data, and then obtain the changed pseudosample labels according to the adaptive threshold. Compared with SRWD and BD, SSIM is a more straightforward way to gauge the areas with higher similarity in PolSAR data (i.e., unchanged regions). In this article, SSIM is mainly used to obtain similarity maps between PolSAR data of dual time series, and then obtain unchanged pseudosample labels according to adaptive thresholds.

B. Pseudolabeled Samples Obtaining

To make full use of full-polarization and dual-polarization data for a more accurate change detection, this paper first obtains three kinds of distance measure maps based on three similarity metrics. This section is mainly based on the three distance measure maps combined with adaptive thresholds to obtain more reliable pseudochanged and unchanged samples. The pseudolabel obtaining method must simultaneously meet the following conditions: unsupervised manner, visualizable, with generalization, and have a certain correlation with real changes areas. Based on the above three distance measure maps, this section uses the process shown in Fig. 3 to obtain reliable pseudosamples, mainly including feature distribution equalization, threshold selection, and postprocessing.

Specifically, due to the distribution characteristics of PolSAR data, there is also a significant uneven statistical distribution problem in the obtained distribution of original PolSAR distance measurements. First, the linear function normalization method of optimizing the maximum and minimum values is applied to normalize the distance measure maps, which is convenient for visualization and subsequent threshold selections. Second, for the normalized measure maps SRWD and BD, we set a threshold based on 1.5 times of the mean value, and the areas with measure values higher than this threshold as preliminary change samples.

Only the samples that exceed the thresholds in both normalized SRWD and BD maps are selected as pseudochange samples. For the normalized SSIM measure maps, we set a threshold of 0.5 times the mean value, and the areas with measure values lower than this threshold as preliminary nonchange samples. For the obtained initial changes and nonchange samples, combined with morphological postprocessing, small and fragmented areas are removed. After normalization, threshold selection, and postprocessing, the changed and unchanged samples are combined to form pseudochanged samples. As shown in the right of Fig. 3, there are many regions still undetermined in the pseudosample maps. Further judgment needs to be made in conjunction with subsequent networks. The selected two types of pseudosamples are used as accurate labeled samples for subsequent ConvLSTM network input to time-series PolSAR data, and the pseudo samples and network is applied for efficient change detection. It is not necessary to obtain too many pseudosamples in this step, but the accuracy of the obtained changed and unchanged pseudosamples is required to be high.

C. Applied ConvLSTM Architecture

Based on the pseudolabels obtained from Section III-B, combined with the T_3 coherence matrices of temporal PolSAR and the distance measure maps obtained from Section III-A, these multidimensional features and limited pseudolabels are used as inputs for training the ConvLSTM network. The applied ConvLSTM architecture is shown in Fig. 4, which combines convolutional operations that can extract spatial features with LSTM networks that can extract temporal features. Introducing ConvLSTM network into time-series PolSAR change detection has advantages in multidimensional data processing with spatial information sequences. This ConvLSTM network is a supervised network, we trained the model using 5% of the selected pseudosamples. Considering the superior performance of this network for limited number of samples and the needs of multidimensional inputs, we chose this robust ConvLSTM to detect the change and nonchange regions of time-series SAR. The network

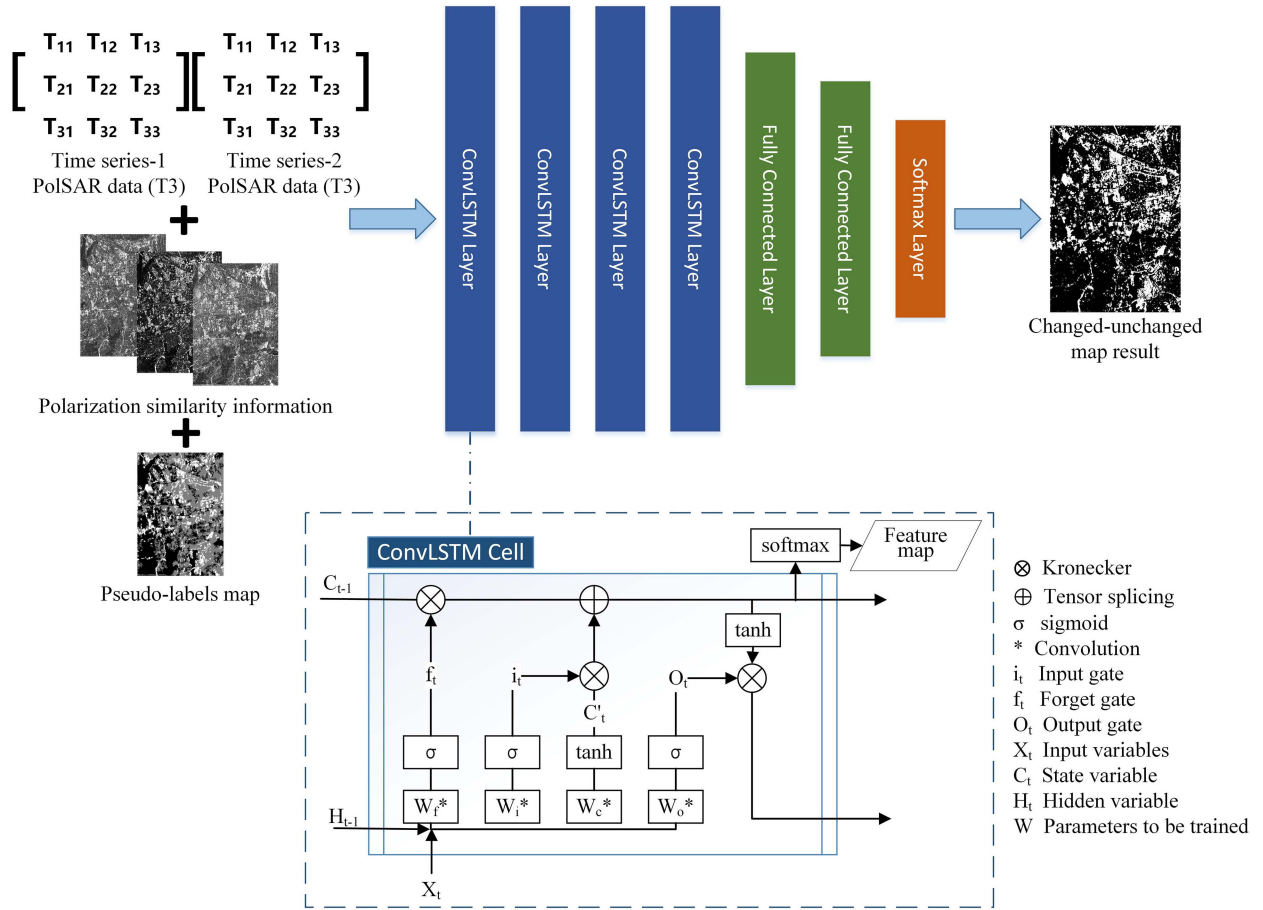


Fig. 4. Applied ConvLSTM architecture.

parameter settings and specific effects of parameters, and sample proportion will be further discussed in the Sections V-B and C. Although this article uses the supervised learning network, the obtained pseudosamples are automatically generated without manual participation. Therefore, the proposed method should be categorized as an unsupervised method, fitting to the massive unlabeled temporal SAR change detection tasks.

IV. EXPERIMENTAL AND RESULTS

The applied datasets, experimental settings, and comparative experiments are introduced in this section. Then, the proposed PDM-ConvLSTM are verified. Moreover, further comparisons and discussion are presented.

A. Experimental Datasets and Settings

The effectiveness of the proposed method was tested on three Radarsat-2 spaceborne PolSAR data, two Sentinel-1 spaceborne PolSAR data, and two UAVSAR airborne PolSAR data. The basic information of selected dataset is shown in Table I. As shown in Figs. 5, 6, and 7, these three groups of datasets include typical land-cover changes such as changes in urban expansion, changes in water bodies, and changes in vegetation types. For the Radarsat-2 dataset and open-source UAVSAR [32], [33]

dataset, there are corresponding labeled Ground Truths (GT) with changed areas that can be used for validation. For the Sentinel-1 dataset, only part of GTs is available.

It should be noted that the proposed method in the article belongs to unsupervised methods and does not require labeled samples for training. The selection of pseudosamples is based on unsupervised approach. The manually annotated GT used in this article are all used for accuracy verification and partial comparative experiments. For the proposed PDM-ConvLSTM, the ratio of pseudosamples is set as 5% by default in an unsupervised manner. Based on the selected reliable pseudosamples, combining with ConvLSTM network, the change detection results can be obtained. The rationality of setting the ratio of pseudosamples will be further demonstrated in Section IV-C.

As the comparisons of proposed method, the following methods are applied to provide benchmark experimental groups.

1) *Traditional Methods*. ① *Unsupervised – Information-theoretic divergence change detection (ITD-CD)* [34], [35]: Based on the polarimetric coherence matrix of time series PolSAR, unsupervised ITD-CD combined with information-theoretic divergence and constant false alarm rate detection, the change areas of time-series PolSAR can be obtained.

② *Unsupervised – Polarimetric entropy theory change detection (PET-CD)* [36]: Based on the polarimetric covariance

TABLE I
DETAILED INFORMATION OF APPLIED TIME-SERIES POLSAR DATA

Dataset	Sensor-polarization	Imaging Area-Time	Resolution (m) [Range×Azimuth]	Image size (in pixel)	Main types of land cover	Change GT
Rs2-WH-2011	Radarsat-2 Full-polarized	Wuhan, China, 2011-12	12 × 8	2450×3500	Building, vegetation, water, and bare land	Contains change GT for verification
Rs2-WH-2015	Radarsat-2 Full-polarized	Wuhan, China, 2015-06	12 × 8	2450×3500	Building, vegetation, water, and bare land	
Rs2-WH-2016	Radarsat-2 Full-polarized	Wuhan, China, 2016-07	12 × 8	2450×3500	Building, vegetation, water, and bare land	
UAVSAR-LA-2009	UAVSAR Full-polarized	Los Angeles, USA, 2009-04	0.5× 1.6	300×786	Building and vegetation	Contains change GT for verification
UAVSAR-LA-2015	UAVSAR Full-polarized	Los Angeles, USA, 2015-05	0.5× 1.6	300×786	Building and vegetation	
S1-XA-2015	Sentinel-1 Dual-polarized	Xi'an, China, 2015-12	20×22	9892×5100	Building, vegetation, water, mountains	Contains partial change GT for comparison
S1-XA-2021	Sentinel-1 Dual-polarized	Xi'an, China, 2021-12	20×22	9892×5100	Building, vegetation, water, mountains	

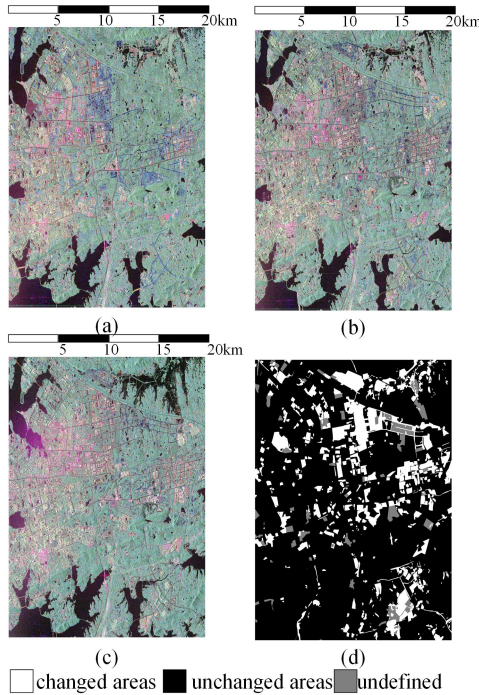


Fig. 5. Rs2-WH dataset: (a) Pauli RGB image of Rs2-WH-2011; (b) Pauli RGB image of Rs2-WH-2015; (c) Pauli RGB image of Rs2-WH-2016; (d) change GT map of Rs2-WH-2011-2015.

matrix of time series PolSAR, unsupervised PET-CD combined with the entropy images and user-defined thresholds to obtain change information of time series data.

2) *Deep Learning Methods*. ① *Unsupervised – Convolutional-wavelet neural networks (CWNN) [20]*: Wavelet transform is introduced into unsupervised multitemporal SAR CWNN change detection to reduce the effect of speckle noise. The CWNN can effectively exploit change information from multitemporal images.

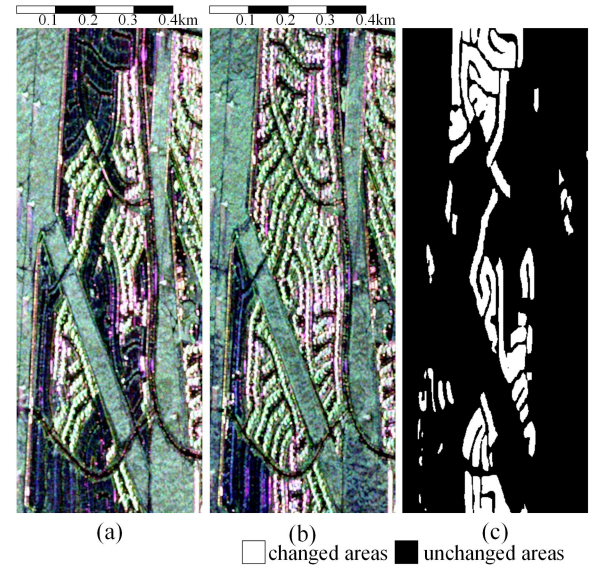


Fig. 6. (a) Pauli RGB image of UAVSAR-LA-2009. (b) Pauli RGB image of UAVSAR-LA-2015. (c) Change GT map of UAVSAR-LA-2009-2015.

② *Unsupervised – Fully Convolutional Change Detection Framework with Generative Adversarial Network (FCD-GAN) [37]*: FCD-GAN is a newly proposed framework for change detection in multitemporal remote sensing images. The iterative optimization of Unet segmentor and image-to-image generator can build a network for unsupervised multitemporal image change detection.

③ *Supervised – Convolutional Long Short Term Memory (ConvLSTM) [38]*: The end-to-end supervised ConvLSTM network is used to learn the deep mutual information of polarimetric coherent matrices in the rotation domain with different polarimetric orientation angles for PolSAR image change detection.

For the above comparison methods, the applied features are generally the nine elements of coherence matrix or the three

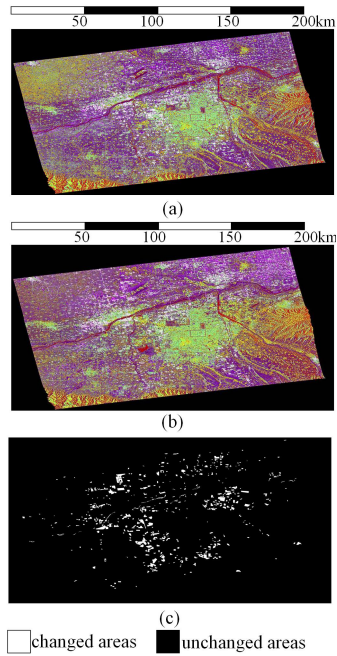


Fig. 7. (a) Pseudocolor image of S1-XA-2015. (b) Pseudocolor image of S1-XA-2021. (c) Change GT map of S1-XA-2015-2021.

diagonal elements of polarimetric coherence matrix. The unsupervised comparison method does not need labeled samples, while the supervised comparison method sets 5% of the labeled samples. The proposed unsupervised PDM-ConvLSTM also applied 5% pseudosamples for training. The selections of samples are all randomized.

B. Experimental Results

To validate the proposed PDM-ConvLSTM, this section first presents the results of key steps, including similarity maps, pseudolabel maps, and change detection results. The similarity maps are the foundation, and the pseudolabel maps are the key to the effectiveness of PDM-ConvLSTM. By combining ConvLSTM network and the accurate pseudosamples, the change detection results can be obtained. Taking the Rs2-WH-2011/Rs2-WH-2015 dataset as an example, Figs. 8 and 9 show the similarity maps, pseudolabel maps. From Fig. 8, it can be seen that the pseudosamples selected through PDMs visualization and thresholds are not many in quantity, and only a portion of these pseudosamples will be selected to participate in network training. In the subsequent discussion section, the reliability of these pseudosamples will be evaluated in multiple aspects through change detection accuracies and direct comparisons with annotations.

In addition, the change detection results of the UAVSAR-LA-2009/UAVSAR-LA-2015, S1-XA-2015/S1-XA-2021, and Rs2-WH-2011/Rs2-WH-2016 datasets are shown in the Figs. 10, 11, 12, and 13, respectively.

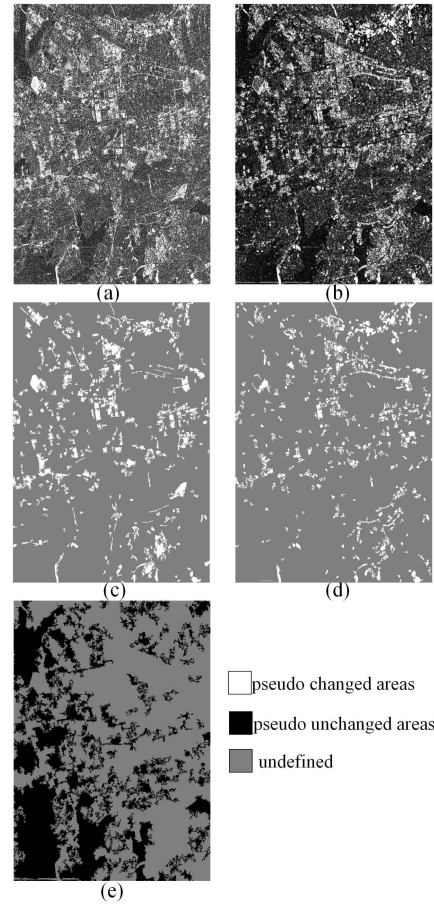


Fig. 8. Similarity map and pseudosamples map of Rs2-WH-2011/2015 dataset. (a) SRWD+BD map. (b) SSIM map. (c) Changed pseudolabels generated by SRWD+BD map. (d) Changed pseudolabels generated by SSIM map. (e) Unchanged pseudolabels generated by SSIM map.

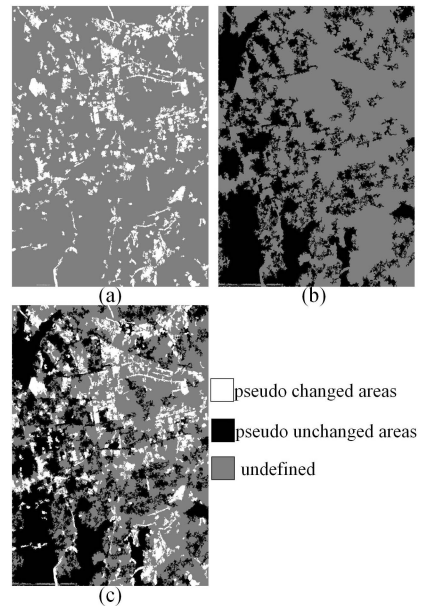


Fig. 9. Pseudolabels map of Rs2-WH-2011/Rs2-WH-2015 dataset. (a) changed pseudolabels map. (b) Unchanged pseudolabels map. (c) Changed-unchanged pseudolabels map.

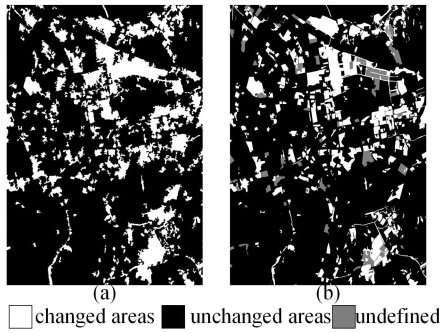


Fig. 10. (a) Change detection result of Rs2-WH-2011-2015 dataset. (b) Corresponding GT map.

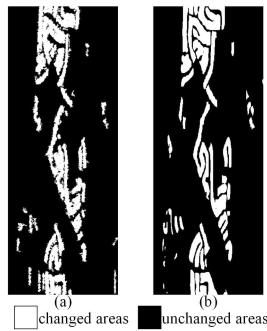


Fig. 11. (a) Change detection result of UAVSAR-LA-2009-2015 dataset. (b) Corresponding GT map.

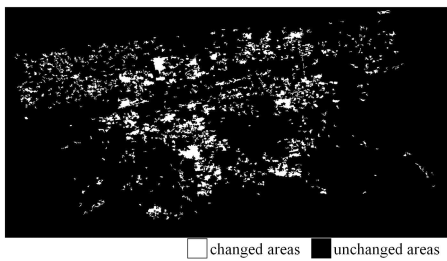


Fig. 12. Change detection result of S1-XA-2015-2021 dataset.

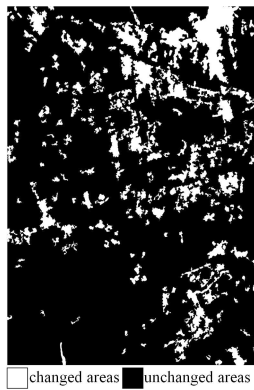


Fig. 13. Change detection result of Rs2-WH-2011-2016 dataset.

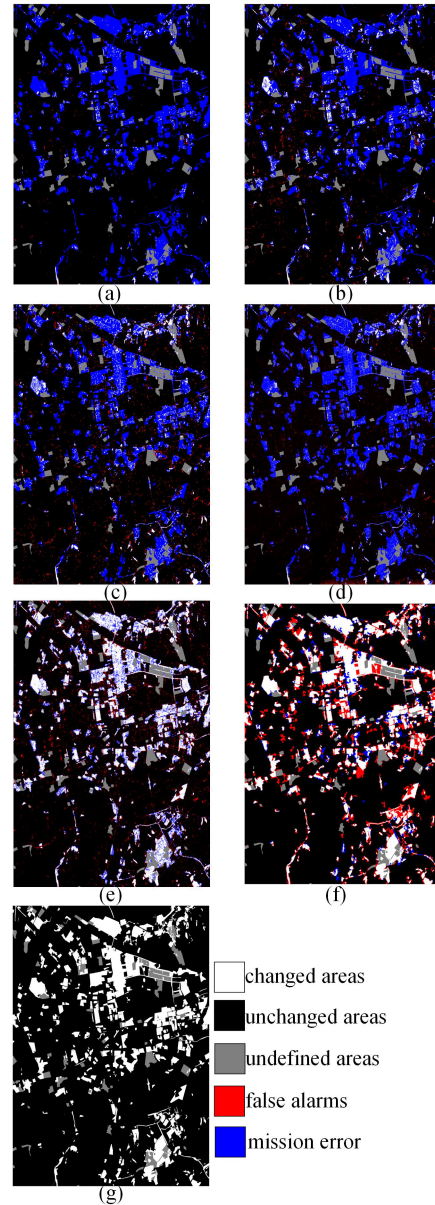


Fig. 14. Change detection results of Rs2-WH-2011-2015 dataset. (a) ITD-CD. (b) PET-CD. (c) CWNN. (d) FCD-GAN. (e) ConvLSTM. (f) PDM-ConvLSTM. (g) GT map.

C. Comparisons and Analysis

Section IV-B provides the change detection results of three groups of applied datasets. It can be seen that the proposed unsupervised PDM-ConvLSTM can detect change regions in time-series PolSAR imageries. To evaluate the method quantitatively, we selected two groups of datasets from Part IV-A and comparative experimental results to quantitatively evaluate and compare the effectiveness and stability of the PDM-ConvLSTM.

Taking datasets Rs2-WH-2011/Rs2-WH-2015 and UAVSAR-LA-2009/UAVSAR-LA-2015 as examples, Figs. 14 and 15 show the comparative experimental results, and the quantitative evaluations are detailed in Tables II and III, respectively. From the results, it can be seen that the

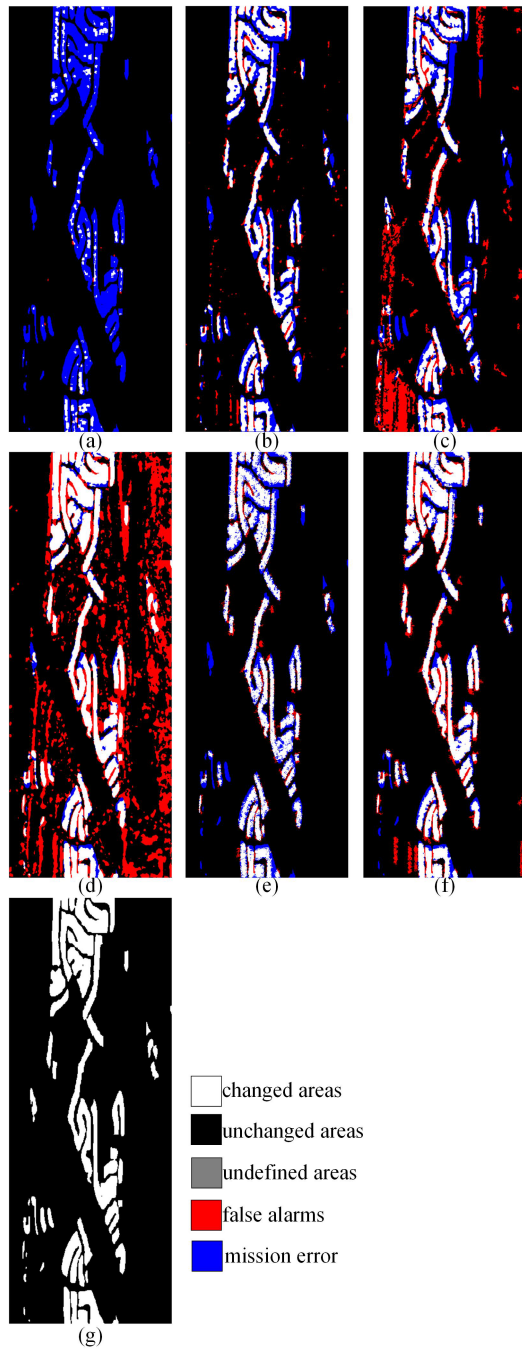


Fig. 15. Change detection results of UAVSAR-LA-2009-2015 dataset. (a) ITD-CD. (b) PET-CD. (c) CWNN. (d) FCD-GAN. (e) ConvLSTM. (f) PDM-ConvLSTM. (g) GT.

quantitative evaluation of the PDM-ConvLSTM on the UAVSAR-LA-2009/2015 dataset is comparable with that of the supervised method under the same sample condition. The quantitative results of two datasets indicate that the proposed method is superior to other unsupervised methods, and has comparability with the results of supervised methods under the same proportion of samples. Multiple quantitative results and comparative results demonstrate the effectiveness and stability of the proposed PDM-ConvLSTM.

TABLE II
QUANTITATIVE EVALUATIONS OF RESULTS ON RS2-WH-2011-2015 DATASET

Methods	OA*	KC	Pre	Rec	F1
ITD-CD	0.8405	0.0782	0.8145	0.0512	0.0963
PET-CD	0.8472	0.1950	0.6861	0.1470	0.2422
CWNN	0.8444	0.2130	0.6096	0.1743	0.2711
FCD-GAN	0.8287	0.1387	0.4465	0.1323	0.2041
ConvLSTM	0.9194	0.7028	0.7715	0.7312	0.7508
PDM-ConvLSTM	0.8959	0.6663	0.6420	0.8439	0.7292

* *OA*: overall accuracy; *KC*: Kappa coefficient; *Pre*: precision rate; *Rec*: recall rate; *F1*: F1-score, which is the weighted harmonic mean of precision rate and recall rate.

The bold entities indicate the highest or prominent values.

TABLE III
QUANTITATIVE EVALUATIONS OF RESULTS ON UAVSAR-LA-2009-2015 DATASET

Methods	OA	KC	Pre	Rec	F1
ITD-CD	0.8625	0.1851	0.9627	0.1198	0.2131
PET-CD	0.9201	0.6641	0.8164	0.6272	0.7094
CWNN	0.8749	0.5242	0.5973	0.5993	0.5983
FCD-GAN	0.8058	0.4762	0.4379	0.8805	0.5849
ConvLSTM	0.9155	0.6170	0.8749	0.5325	0.6620
PDM-ConvLSTM	0.9324	0.7445	0.7775	0.7918	0.7846

The bold entities indicate the highest or prominent values.

V. DISCUSSIONS

To further demonstrate the rationality of applied PDM, pseudosamples and network, as well as the sensitivity and limitations of the proposed method. This section uses comparative experiments and quantitative evaluations to discuss the rationality of the selected PDM, the rationality of the selected network and network parameters, the accuracy and impact of pseudosamples proportional, and the qualitative analysis of the local regions of interest in change detection results.

A. Discussions About Rationality of the Selected PDMs

The comparisons in Tables II and III illustrate the effectiveness of the three selected PDMs, but their superiority over other distance measures has not been compared. Based on the UAVSAR-LA-2009-2015 dataset, we supplemented the discussion on the experimental effects of other typical distance measures, including Bregman divergence, Jensen Shannon divergence, revised Wishart distance, Wishart distance, mean squared error/MSE, and cosine similarity. And combined with the contrasting results in following Table IV, we further demonstrated that the three selected PDMs are preponderant. In above supplementary experiments about other distances, the applied pseudosample proportional and network framework were consistent, the MSE and cosine similarity are common distance measures, while the other measures (including Bregman divergence, Jensen Shannon divergence, revised Wishart distance,

TABLE IV
EVALUATION OF COMPARATIVE RESULTS BASED ON DIFFERENT DISTANCE MEASURES

Different distances	OA	KC	Pre	Rec	F1
Bregman divergence	0.6255	0.2704	0.2890	0.9657	0.4449
Jensen Shannon divergence	0.5376	0.1122	0.2105	0.7181	0.3256
revised Wishart distance	0.6939	0.3397	0.3315	0.9535	0.4920
Wishart distance	0.6599	0.2650	0.2929	0.8404	0.4344
MSE+SSIM	0.8994	0.6650	0.6306	0.8523	0.7249
Cosine similarity+SSIM	0.9222	0.7126	0.7324	0.7874	0.7589
Only SRWD	0.8822	0.6333	0.5783	0.8949	0.7026
Only BD	0.7359	0.3960	0.3672	0.9659	0.5321
Only SSIM	0.9160	0.7059	0.6893	0.8372	0.7561
SRWD+BD	0.8272	0.5306	0.4719	0.9368	0.6277
SRWD+SSIM	0.9093	0.6929	0.6594	0.8613	0.7470
BD+SSIM	0.8991	0.6713	0.6239	0.8832	0.7312
Applied PDMs	0.9324	0.7445	0.7775	0.7918	0.7846

The bold entities indicate the highest or prominent values.

Wishart distance) were classical measures suitable for describing PolSAR data. Due to the influence of SAR speckle and the particularity of polarimetric distributions, not all typical distance measurements suitable to be applied for pseudosamples selection in this method. The three adopted PDMs in the proposed framework utilize the distribution characteristics of PolSAR data and the similarity of PolSAR image structures. Compared to other typical distance measures, they are more suitable for the accuracy of unsupervised PolSAR change detection.

In addition, in order to further improve the ablation experiments, we also conducted supplementary experiments by comparing a single distance and any combination of two distances for the three applied PDMs in Table IV.

B. Discussions About Rationality of the Selected Network and Network Parameters

After obtaining the three distance measures, the nine-dimensional polarimetric coherence matrix features of two time series PolSAR are combined. And these high-dimensional features are input to the network for deep learning model training and testing. These high-dimensional data input has high requirements for network selection. And in addition, due to the limited number of pseudosamples, there are also high requirements for the applied network. Thus, considering the requirements of multidimensional input and limited samples (with imbalanced change/unchanged class samples), we select the convLSTM model. Although the motivations of selected convLSTM is not novel enough, this model has strong robustness and scalability. In addition, to demonstrate the suitability of convLSTM for the proposed method, we further compared the change detection results using other networks combined with the obtained pseudosamples. Based on the UAVSAR-LA-2009-2015 dataset, we supplemented the experimental effects of other typical networks (including VGG and Vision Transformer/ViT [39]). The results are shown in Table V, these can further demonstrate that the

TABLE V
EVALUATION OF COMPARATIVE RESULTS OF SUPPLEMENTING TYPICAL NETWORKS AND CONVLSTM PARAMETER ANALYSIS

Different networks and parameters	OA	KC	Pre	Rec	F1
VGG	0.9235	0.7359	0.7024	0.8810	0.7816
ViT	0.9214	0.7295	0.6959	0.8782	0.7765
ConvLSTM (Default parameters)	0.9324	0.7445	0.7775	0.7918	0.7846
ConvLSTM (hidden_dim=6)	0.9328	0.7480	0.7739	0.8025	0.7839
ConvLSTM (hidden_dim=20)	0.9319	0.7464	0.7659	0.8092	0.7870
ConvLSTM (num_layers=3)	0.9307	0.7452	0.7554	0.8203	0.7865
ConvLSTM (num_layers=5)	0.9230	0.7292	0.7099	0.8539	0.7753

The bold entities indicate the highest or prominent values.

applied convLSTM has advantages, especially in high-dimensional input and limited samples.

Furthermore, for the applied ConvLSTM network architecture in this paper, the default parameters are: the learning rate is set to 0.001, the Epochs is set to 200, the batch size is set to 128, the activation function is set to ReLu and the optimizer is set to SGD (Stochastic Gradient Descent), the number of the middle layer (hidden_Dim) is set to 10, the number of network cells (num_Layers) is set to 1. The purpose of ConvLSTM training is to update parameters and optimize the objective function. The applied SGD calculates a local estimate based on the data of each batch, minimizing the cost function. The SGD results are more reliable with good initialization and learning rate scheduling scheme. The learning rate determines the size of each step. To further demonstrate the rationality of the applied network parameters, we analyzed some network hyperparameters, including the adjustment of the network hidden_Dim, num_Layers, as shown in following Table V. Among them, increasing the number of LSTM cells will increase significant time cost.

Considering the balance between accuracy and training time cost, the applied network parameters are mainly implemented based on experience and by default. The comparative evaluations of results under different network parameters are shown in Table V, these also proves that the selected parameter settings are feasible.

C. Accuracy and Proportional Impact of Pseudosamples

For the proposed method, the accuracy of pseudosamples is the core, this section demonstrates the accuracy of selected pseudosamples and the rationality of the proportion of applied pseudolabeled samples through two comparative experiments. First, we directly evaluate the accuracy of the pseudosamples through labeled GTs of Rs2-WH-2011-2015/ UAVSAR-LA-2009-2015 dataset, based on the accuracy of for all pseudosamples and 5% of the selected pseudosamples. In Table VI, from the evaluated results of pseudosamples and change and nonchange GTs, it can be seen that not all pseudosamples are accurate. However, the strategy of using 5% pseudosamples has achieved an average accuracy of 94.50–95.31% in labeled GTs. Based on these

TABLE VI
EVALUATIONS OF MATCHING ACCURACY BETWEEN SELECTED PSEUDOSAMPLES AND THE LABELED CHANGE/NONCHANGE GTs

Evaluated pseudo samples	Pre_change*	Pre_unchange	Average_pre
All pseudo samples of UAVSAR dataset	0.8418	0.9704	0.9330
All pseudo samples of Rs2-WH-2011-2015 dataset	0.7823	0.9710	0.9367
5% pseudo samples of UAVSAR dataset	0.8529	0.9714	0.9450
5% pseudo samples of Rs2-WH-2011-2015 dataset	0.8241	0.9806	0.9531

***Pre_change**: precision rate of the change pseudo samples and the labeled change GTs; **Pre_unchange**: precision rate of the unchange pseudo samples and the labeled unchange GTs; **Average_Pre**: average precision rate of the selected pseudo samples and the labeled GTs.

The bold entities indicate the highest or prominent values.

TABLE VII
PROPORTION OF PSEUDOLABELED SAMPLES AND THE IMPACT ON THE ACCURACY OF CHANGE DETECTION

Proportion	OA	KC	Pre	Rec	F1
2%	0.9279	0.7322	0.7524	0.7992	0.7751
5%	0.9324	0.7445	0.7775	0.7918	0.7846
10%	0.9290	0.7403	0.7468	0.8221	0.7826

The bold entities indicate the highest or prominent values.

experiments, it can be demonstrated that the pseudosamples and selection strategies in this paper are reliable. However, in reality, labeled GTs are difficult to obtain or unavailable. The pseudosamples obtained by proposed method can greatly guarantee samples' quality. On the other hand, from Table VI, it can be seen that there is serious class imbalance between the number of change and nonchange pixels in the real datasets. For the UAVSAR dataset, the ratio of change and nonchange pixels is 1:3.6767, and for the Radarsat-2 dataset, the ratio of change and nonchange pixels is 1:4.5245. This imbalance phenomenon also provides certain limitations and motivations for the selection of network models.

Second, we further analyzed the proportion of pseudolabeled samples and the impact on the accuracy of change detection, to demonstrate the sensitivity and limitations of the PDM-ConvLSTM. We carried out the unsupervised change detection under the pseudolabeled sample rate of 2%, 5%, and 10% for the applied UAVSAR datasets. The accuracy evaluation is shown in the following Table VII and Fig. 16. From the comparisons, when the pseudolabeled sample rate is only 2%, the effect of change detection is not satisfying enough than that of 5%. Upon the rising rate of randomized pseudolabeled sample of 10%, the recall metric is enhanced. However, other metrics may degrade than that achieved at 5% sample rate. This is because there may be some inaccurate pseudosamples mixed in the applied samples, and the selection of pseudosamples is random. Therefore, from the perspective of the balance between the training cost and the accuracy, we choose 5% of pseudolabeled samples for model training and change detections.

Analysis of differences in sample size ratio

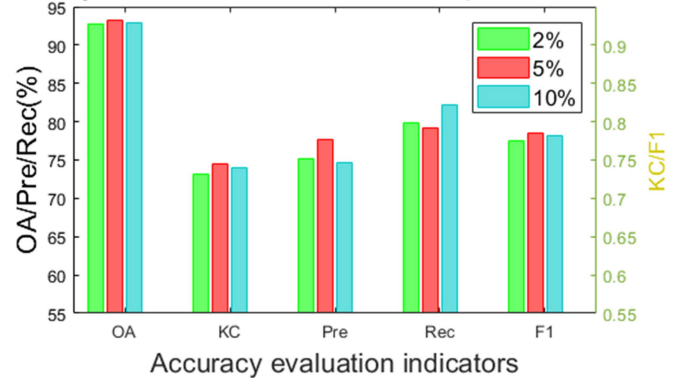


Fig. 16. Evaluation of PDM-ConvLSTM under different rates of pseudolabeled sample.

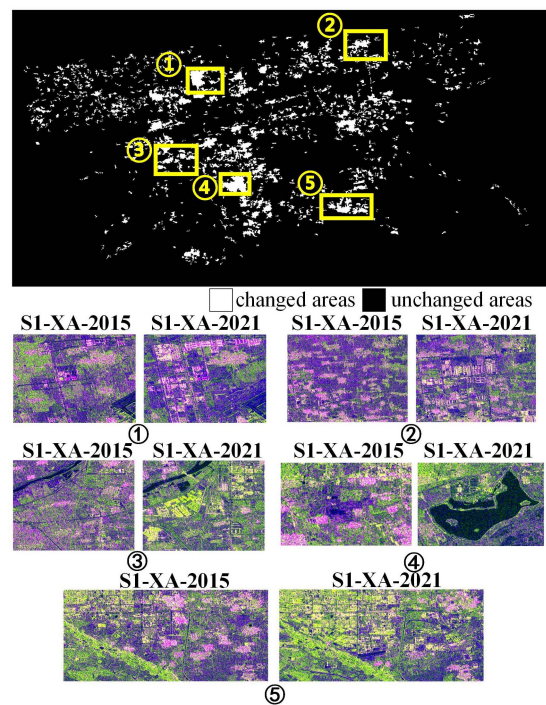


Fig. 17. Local regions of interest in S1-XA-2015-2021 change detection results.

D. Qualitative Analysis of the Local Regions of Interest in Change Detection Results

At last, the robustness and effectiveness of the PDM-ConvLSTM are further qualitatively analyzed by the local regions of the change detection results. The local regions of interest in the results of S1-XA-2015-2021 and Rs2-WH-2011-2016 are shown as following Figs. 17 and 18. From the local comparison results, the proposed PDM-ConvLSTM can detect possible changing regions on time-series unlabeled SAR images, including identifying the mutual changes between water bodies, buildings, vegetation, and bare land. Due to the lack of labeled annotation for accuracy evaluation of the changed areas in these S1-XA-2015-2021 and Rs2-WH-2011-2016 datasets, verifying

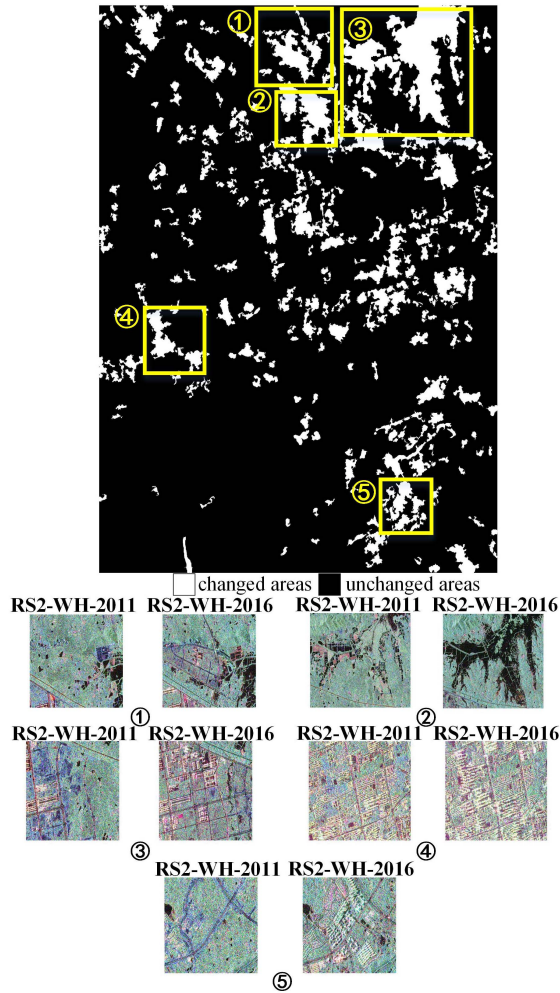


Fig. 18. Local regions of interest in Rs2-WH-2011-2016 change detection results.

the change detection results through local regions can also demonstrate the effectiveness.

However, due to the sensitivity of polarimetric features, it can be seen that the change detection rate of the PDM-ConvLSTM is relatively high, from quantitative and qualitative evaluations. This is mainly due to the detected change areas being larger than the labeled GT, and some unlabeled changes have been detected. These also indicate that polarimetric features can capture some intraclass changes, such as changes in the renovation of building areas and changes in the growth of vegetation areas. At present, the method in this article only uses polarimetric features and deep learning to detect the changing regions, belonging to the binary change detection method. The following research will further explore the polarimetric features to express detail and typical land-cover change types, and focus on utilizing polarimetric features and deep learning to quickly track and analyze specific types of land-cover changes in time-series PolSAR images.

VI. CONCLUSION

An unsupervised change detection method for PolSAR data based on PDM and ConvLSTM, namely PDM-ConvLSTM, is proposed in this article. The pseudosamples obtained based on

multiple polarimetric distance measures can enable the proposed PDM-ConvLSTM to reduce the dependence on labeled samples and the combination of pseudosamples and deep learning can balance the efficiency and accuracy of unsupervised change detection for time series PolSAR images. There are two highlights for the proposed PDM-ConvLSTM method: first, three selected PDMs are utilized to obtain similarity and dis-similarity maps of time-series PolSAR and changed/unchanged pseudosamples, which are suitable for PolSAR distribution characteristics and have the potential to reflect PolSAR changes. This approach aids in mitigating the labor burden for manual annotation. Second, by combining selected reliable pseudosamples with efficient LSTM networks, unsupervised PDM-ConvLSTM does not require additional manual labeled samples, but also attains comparable the efficiency and accuracy as the supervised methods. The sufficient unsupervised experiments and comparisons demonstrate the effectiveness of the PDM-ConvLSTM. The unsupervised change detection accuracy can reach 89.59%–93.24% and is relatively robust. This indicates that the pseudosamples obtained by PDM are reliable. Sufficient comparative experiments, including results from different methods, different distances, different network parameters, and different sample ratios, further demonstrating the effectiveness and reliability of the unsupervised PDM-ConvLSTM. The future work will focus on using similarity maps to measure and track the specific types of land-cover changes in long-time PolSAR series.

ACKNOWLEDGMENT

The authors would like to thank Remote Sensing Laboratory, School of Surveying and Geospatial Engineering, University of Tehran for providing the UAVSAR PolSAR dataset, also like to thank the editor, associate editor, and anonymous reviewers for their constructive and helpful comments that greatly improved this article. Moreover, the authors would also like to thank Dr. Lei Xie in Central South University for proofreading this manuscript.

REFERENCES

- [1] O. Yousif and Y. Ban, "Improving SAR-based urban change detection by combining MAP-MRF classifier and nonlocal means similarity weights," *IEEE J. Sel. Topics Appl. Earth Observ. Remote Sens.*, vol. 7, no. 10, pp. 4288–4300, Oct. 2014, doi: [10.1109/JSTARS.2014.2347171](https://doi.org/10.1109/JSTARS.2014.2347171).
- [2] S. Zhu, Y. Song, Y. Zhang, and Y. Zhang, "ECFNet: A siamese network with fewer FPs and fewer FNs for change detection of remote-sensing images," *IEEE Geosci. Remote Sens. Lett.*, vol. 20, 2023, Art. no. 6001005, doi: [10.1109/LGRS.2023.3238553](https://doi.org/10.1109/LGRS.2023.3238553).
- [3] J. Zhou, M. Li, X. Wang, X. Xiu, and D. Huang, "Extracting tobacco planting areas using LSTM from time series Sentinel-1 SAR data," in *Proc. 9th Int. Conf. Agro-Geoinformatics*, 2021, pp. 1–4, doi: [10.1109/Agro-Geoinformatics50104.2021.9530349](https://doi.org/10.1109/Agro-Geoinformatics50104.2021.9530349).
- [4] M. Khurana and V. Saxena, "A unified approach to change detection using an adaptive ensemble of extreme learning machines," *IEEE Geosci. Remote Sens. Lett.*, vol. 17, no. 5, pp. 794–798, May 2020, doi: [10.1109/LGRS.2019.2933906](https://doi.org/10.1109/LGRS.2019.2933906).
- [5] J. Lu, J. Li, G. Chen, L. Zhao, B. Xiong, and G. Kuang, "Improving pixel-based change detection accuracy using an object-based approach in multitemporal SAR flood images," *IEEE J. Sel. Topics Appl. Earth Observ. Remote Sens.*, vol. 8, no. 7, pp. 3486–3496, Jul. 2015, doi: [10.1109/JSTARS.2015.2416635](https://doi.org/10.1109/JSTARS.2015.2416635).
- [6] Y. Sun, L. Lei, X. Li, X. Tan, and G. Kuang, "Structure consistency-based graph for unsupervised change detection with homogeneous and heterogeneous remote sensing images," *IEEE Trans. Geosci. Remote Sens.*, vol. 60, 2022, Art. no. 4700221, doi: [10.1109/TGRS.2021.3053571](https://doi.org/10.1109/TGRS.2021.3053571).

- [7] G. Moser, S. Serpico, and G. Vernazza, "Unsupervised change detection from multichannel SAR images," *IEEE Geosci. Remote Sens. Lett.*, vol. 4, no. 2, pp. 278–282, Apr. 2007, doi: [10.1109/LGRS.2007.890549](https://doi.org/10.1109/LGRS.2007.890549).
- [8] X. Zhang, X. Su, Q. Yuan, and Q. Wang, "Spatial-temporal gray-level co-occurrence aware CNN for SAR image change detection," *IEEE Geosci. Remote Sens. Lett.*, vol. 19, 2022, Art. no. 4018605, doi: [10.1109/LGRS.2021.3110302](https://doi.org/10.1109/LGRS.2021.3110302).
- [9] Y. Li, C. Peng, Y. Chen, L. Jiao, L. Zhou, and R. Shang, "A deep learning method for change detection in synthetic aperture radar images," *IEEE Trans. Geosci. Remote Sens.*, vol. 57, no. 8, pp. 5751–5763, Aug. 2019, doi: [10.1109/TGRS.2019.2901945](https://doi.org/10.1109/TGRS.2019.2901945).
- [10] H. Dong et al., "Deep shearlet network for change detection in SAR images," *IEEE Trans. Geosci. Remote Sens.*, vol. 60, 2022, Art. no. 5241115, doi: [10.1109/TGRS.2022.3228776](https://doi.org/10.1109/TGRS.2022.3228776).
- [11] J. Zhang, M. Xing, G.-C. Sun, and X. Shi, "Vehicle trace detection in two-pass SAR coherent change detection images with spatial feature enhanced unet and adaptive augmentation," *IEEE Trans. Geosci. Remote Sens.*, vol. 60, 2022, Art. no. 5232415, doi: [10.1109/TGRS.2022.3194903](https://doi.org/10.1109/TGRS.2022.3194903).
- [12] Y. Gao, F. Gao, J. Dong, and H.-C. Li, "SAR image change detection based on multiscale capsule network," *IEEE Geosci. Remote Sens. Lett.*, vol. 18, no. 3, pp. 484–488, Mar. 2021, doi: [10.1109/LGRS.2020.2977838](https://doi.org/10.1109/LGRS.2020.2977838).
- [13] T. Bai et al., "Deep learning for change detection in remote sensing: A review," *Geo-Spatial Inf. Sci.*, pp. 1–27, 2022, doi: [10.1080/10095020.2022.2085633](https://doi.org/10.1080/10095020.2022.2085633).
- [14] L. Khelifi and M. Mignotte, "Deep learning for change detection in remote sensing images: Comprehensive review and meta-analysis," *IEEE Access*, vol. 8, pp. 126385–126400, 2020, doi: [10.1109/ACCESS.2020.3008036](https://doi.org/10.1109/ACCESS.2020.3008036).
- [15] S. Saha, F. Bovolo, and L. Bruzzone, "Building change detection in VHR SAR images via unsupervised deep transcoding," *IEEE Trans. Geosci. Remote Sens.*, vol. 59, no. 3, pp. 1917–1929, Mar. 2021, doi: [10.1109/TGRS.2020.3000296](https://doi.org/10.1109/TGRS.2020.3000296).
- [16] Y. Wang, L. Du, and H. Dai, "Unsupervised SAR image change detection based on SIFT keypoints and region information," *IEEE Geosci. Remote Sens. Lett.*, vol. 13, no. 7, pp. 931–935, Jul. 2016, doi: [10.1109/LGRS.2016.2554606](https://doi.org/10.1109/LGRS.2016.2554606).
- [17] T. Celik, "Unsupervised change detection in satellite images using principal component analysis and k -means clustering," *IEEE Geosci. Remote Sens. Lett.*, vol. 6, no. 4, pp. 772–776, Oct. 2009, doi: [10.1109/LGRS.2009.2025059](https://doi.org/10.1109/LGRS.2009.2025059).
- [18] H. Zhang, M. Gong, P. Zhang, L. Su, and J. Shi, "Feature-level change detection using deep representation and feature change analysis for multispectral imagery," *IEEE Geosci. Remote Sens. Lett.*, vol. 13, no. 11, pp. 1666–1670, Nov. 2016, doi: [10.1109/LGRS.2016.2601930](https://doi.org/10.1109/LGRS.2016.2601930).
- [19] Y. Gao, F. Gao, J. Dong, and S. Wang, "Change detection from synthetic aperture radar images based on channel weighting-based deep cascade network," *IEEE J. Sel. Topics Appl. Earth Observ. Remote Sens.*, vol. 12, no. 11, pp. 4517–4529, Nov. 2019, doi: [10.1109/JSTARS.2019.2953128](https://doi.org/10.1109/JSTARS.2019.2953128).
- [20] F. Gao, X. Wang, Y. Gao, J. Dong, and S. Wang, "Sea ice change detection in SAR images based on convolutional-wavelet neural networks," *IEEE Geosci. Remote Sens. Lett.*, vol. 16, no. 8, pp. 1240–1244, Aug. 2019, doi: [10.1109/LGRS.2019.2895656](https://doi.org/10.1109/LGRS.2019.2895656).
- [21] N. Lv, C. Chen, T. Qiu, and A. K. Sangaiah, "Deep learning and superpixel feature extraction based on contractive autoencoder for change detection in SAR images," *IEEE Trans. Ind. Inform.*, vol. 14, no. 12, pp. 5530–5538, Dec. 2018, doi: [10.1109/TII.2018.2873492](https://doi.org/10.1109/TII.2018.2873492).
- [22] Y. Lei, X. Liu, J. Shi, C. Lei, and J. Wang, "Multiscale superpixel segmentation with deep features for change detection," *IEEE Access*, vol. 7, pp. 36600–36616, 2019, doi: [10.1109/ACCESS.2019.2902613](https://doi.org/10.1109/ACCESS.2019.2902613).
- [23] S. Hochreiter and J. Schmidhuber, "Long short-term memory," *Neural Comput.*, vol. 9, no. 8, pp. 1735–1780, 1997, doi: [10.1162/neco.1997.9.8.1735](https://doi.org/10.1162/neco.1997.9.8.1735).
- [24] C. Wang, X. Liu, J. Pei, Y. Huang, Y. Zhang, and J. Yang, "Multiview attention CNN-LSTM network for SAR automatic target recognition," *IEEE J. Sel. Topics Appl. Earth Observ. Remote Sens.*, vol. 14, pp. 12504–12513, 2021, doi: [10.1109/JSTARS.2021.3130582](https://doi.org/10.1109/JSTARS.2021.3130582).
- [25] Z. Lin, W. Liu, C. Niu, and W. Lu, "Change type recognition for SAR images using statistical bidirectional LSTM network with few labeled samples," *IEEE Geosci. Remote Sens. Lett.*, vol. 19, 2022, Art. no. 4516205, doi: [10.1109/LGRS.2022.3222794](https://doi.org/10.1109/LGRS.2022.3222794).
- [26] X. Qin et al., "Distance measures of polarimetric SAR image data: A survey," *Remote Sens.*, vol. 14, no. 22, 2022, Art. no. 5873, doi: [10.3390/rs14225873](https://doi.org/10.3390/rs14225873).
- [27] K. Ersahin, I. G. Cumming, and R. K. Ward, "Segmentation of polarimetric SAR data using contour information via spectral graph partitioning," in *Proc. IEEE Int. Geosci. Remote Sens. Symp.*, 2007, pp. 2240–2243, doi: [10.1109/IGARSS.2007.4423285](https://doi.org/10.1109/IGARSS.2007.4423285).
- [28] P. R. Kersten, J.-S. Lee, and T. L. Ainsworth, "Unsupervised classification of polarimetric synthetic aperture radar images using fuzzy clustering and EM clustering," *IEEE Trans. Geosci. Remote Sens.*, vol. 43, no. 3, pp. 519–527, Mar. 2005, doi: [10.1109/TGRS.2004.842108](https://doi.org/10.1109/TGRS.2004.842108).
- [29] S. N. Anfinsen, R. Jenssen, and T. Eltoft, "Spectral clustering of polarimetric SAR data with Wishart-derived distance measures," in *Proc. 3rd Int. Workshop Sci. Appl. SAR Polarimetry Polarimetric Interferometry*, Noordwijk, Netherlands, 2007. [Online]. Available: <http://adsabs.harvard.edu/abs/2007ESASP.644E..10A>
- [30] S. Ren and F. Zhou, "Semi-supervised classification of PolSAR data with multi-scale weighted graph convolutional network," in *Proc. IEEE Int. Geosci. Remote Sens. Symp.*, 2020, pp. 1715–1718, doi: [10.1109/IGARSS39084.2020.9324732](https://doi.org/10.1109/IGARSS39084.2020.9324732).
- [31] Z. Wang, A. C. Bovik, H. R. Sheikh, and E. P. Simoncelli, "Image quality assessment: From error visibility to structural similarity," *IEEE Trans. Image Process.*, vol. 13, no. 4, pp. 600–612, Apr. 2004, doi: [10.1109/TIP.2003.819861](https://doi.org/10.1109/TIP.2003.819861).
- [32] A. Najafi and M. Hasanlou, "Land cover changes detection in polarimetric SAR data using algebra, similarity, and distance based methods," *J. Geospatial Inf. Technol.*, vol. 6, pp. 143–163, Sep. 2018, doi: [10.29252/jgit.6.2.143](https://doi.org/10.29252/jgit.6.2.143).
- [33] R. Habibollahi, S. T. Seydi, M. Hasanlou, and M. Mahdianpari, "TCD-Net: A novel deep learning framework for fully polarimetric change detection using transfer learning," *Remote Sens.*, vol. 14, no. 3, 2022, doi: [10.3390/rs14030438](https://doi.org/10.3390/rs14030438).
- [34] H. Song, W. Yang, X. Huang, and X. Xu, "Region-based change detection of PolSAR images using analytic information-theoretic divergence," in *Proc. 8th Int. Workshop Anal. Multitemporal Remote Sens. Images*, 2015, pp. 1–4.
- [35] W. Yang, X. Yang, T. Yan, H. Song, and G.-S. Xia, "Region-based change detection for polarimetric SAR images using wishart mixture models," *IEEE Trans. Geosci. Remote Sens.*, vol. 54, no. 11, pp. 6746–6756, Nov. 2016, doi: [10.1109/TGRS.2016.2590145](https://doi.org/10.1109/TGRS.2016.2590145).
- [36] M. He, X. F. He, and H. B. Luo, "Detection of information change on SAR images based on entropy theory," in *Proc. 1st Asian Pacific Conf. Synthetic Aperture Radar*, 2007, pp. 775–778, doi: [10.1109/APSAR.2007.4418725](https://doi.org/10.1109/APSAR.2007.4418725).
- [37] C. Wu, B. Du, and L. Zhang, "Fully convolutional change detection framework with generative adversarial network for unsupervised, weakly supervised and regional supervised change detection," *IEEE Trans. Pattern Anal. Mach. Intell.*, vol. 45, no. 8, pp. 9774–9788, Aug. 2023, doi: [10.1109/TPAMI.2023.3237896](https://doi.org/10.1109/TPAMI.2023.3237896).
- [38] L. Wang, X. Xu, R. Gui, R. Yang, and F. Pu, "Learning rotation domain deep mutual information using convolutional LSTM for unsupervised PolSAR image classification," *Remote Sens.*, vol. 12, no. 24, 2020, Art. no. 4075, doi: [10.3390/rs12244075](https://doi.org/10.3390/rs12244075).
- [39] H. Dong, L. Zhang, and B. Zou, "Exploring vision transformers for polarimetric SAR image classification," *IEEE Trans. Geosci. Remote Sens.*, vol. 60, 2022, Art. no. 5219715, doi: [10.1109/TGRS.2021.3137383](https://doi.org/10.1109/TGRS.2021.3137383).



Rong Gui received the M.E. and Ph.D. degrees in signal and information processing from Wuhan University, Wuhan, China, in 2016 and 2021, respectively.

She is currently working as a Lecturer with the Department of Geomatics and Remote Sensing, School of Geosciences and Info-Physics, Central South University. Her research interests include SAR imagery processing, multisource fusion algorithms of SAR, 3D laser measurement technology, pattern recognition.



Xinyue Zhang received the B.E. degree in remote sensing science and technology from China University of Geosciences, Wuhan, China, in 2022. She is currently working toward the Postgraduate degree in photogrammetry and remote sensing with Central South University, Changsha, China.

Her research interests include efficient interpretation and change detection of massive temporal SAR data based on deep learning.



Jun Hu (Senior Member, IEEE) received the M.Eng. and Ph.D. degrees in geodesy and surveying engineering from Central South University, Changsha, China, in 2008 and 2013, respectively.

From 2013 to 2014, he was a Postdoctoral Fellow with the Department of Land Surveying and Geo-Informatics, The Hong Kong Polytechnic University, Hong Kong. He is currently a Full Professor with the Department of Geomatics and Remote Sensing, School of Geosciences and Info-Physics, Central South University. He is the author of more than 60 papers in international peer-reviewed journals. His research interests include mapping multidimensional and high-precision deformations under complicated environment and its applications in geophysical fields.



Xing Zhang received the B.S. degree in Surveying and Mapping Engineering from Guizhou University, Guiyang, China, in 2017. He is currently working toward the master's and doctoral postgraduate degree with photogrammetry and remote sensing with Central South University, Changsha, China. His research interests include SAR and interferometric synthetic aperture radar (InSAR) processing and researching on geophysical parameter inversion methods



Lei Wang received the B.S. degree in circuit and system, the M.S. degree in communication engineering, and the Ph.D. degree in signal and information processing from Wuhan University, Wuhan, China, in 2009, 2011, and 2020, respectively.

He is currently a Lecturer with the School of Electrical and Information Engineering, Wuhan Institute of Technology, Wuhan, Hubei, China. His research interests include deep learning and polarimetric SAR image processing.